Research Article | Vol. 27, No. 11 | 27 May 2019 | OPTICS EXPRESS 15205
Optics EXPRESS

Mesoscale laser 3D printing

LINAS JONUŠAUSKAS,[1,2] DARIUS GAILEVIČIUS,[1] SIMA REKŠTYTĖ,[1] TOMMASO BALDACCHINI,[3,7] SAULIUS JUODKAZIS,[4,5,6,8] AND MANGIRDAS MALINAUSKAS[1,6,9]

[1]*Laser Research Center, Physics Faculty, Vilnius University, Saulėtekio Ave. 10, Vilnius LT-10223, Lithuania*
[2]*Femtika Ltd., Saulėtekio Ave. 15, Vilnius LT-10224, Lithuania*
[3]*Schmid College of Science and Technology Chapman University, One University Drive, Orange, CA 92866, USA*
[4]*Center for Micro-Photonics, Faculty of Engineering and Industrial Sciences, Swinburne University of Technology, Hawthorn, Victoria, Australia*
[5]*Melbourne Center for Nanofabrication, Australian National Fabrication Facility, Clayton, Victoria, Australia*
[6]*Tokyo Tech World Research Hub Initiative (WRHI), School of Materials and Chemical Technology, Tokyo Institute of Technology, 2-12-1 Ookayama, Meguro-ku, Tokyo 152-8550, Japan*
[7]*baldacchini@chapman.edu*
[8]*sjuodkazis@swin.edu.au*
[9]*mangirdas.malinauskas@ff.vu.lt*

Abstract: 3D meso scale structures that can reach up to centimeters in overall size but retain micro- or nano-features, proved to be promising in various science fields ranging from micro-mechanical metamaterials to photonics and bio-medical scaffolds. In this work, we present synchronization of the linear and galvanometric scanners for efficient femtosecond 3D optical printing of objects at the meso-scale (from sub-μm to sub-cm spanning five orders of magnitude). In such configuration, the linear stages provide stitch-free structuring at nearly limitless (up to tens-of-cm) working area, while galvo-scanners allow achieving translation velocities in the range of mm/s-cm/s without sacrificing nano-scale positioning accuracy and preserving the undistorted shape of the final print. The principle behind this approach is demonstrated, proving its inherent advantages in comparison to separate use of only linear stages or scanners. The printing rate is calculated in terms of voxels/s, showcasing the capability to maintain an optimal feature size while increasing throughput. Full capabilities of this approach are demonstrated by fabricating structures that reach millimeters in size but still retain sub-μm features: scaffolds for cell growth, microlenses, and photonic crystals. All this is combined into a benchmark structure: a meso-butterfly. Provided results show that synchronization of two scan modes is crucial for the end goal of industrial-scale implementation of this technology and makes the laser printing well aligned with similar approaches in nanofabrication by electron and ion beams.

1. Introduction

The 4th industrial revolution is in full swing, pushing the boundaries of scientific and industrial advances to ever new heights. The key features of this development include the usage of smart devices and methodologies as well as blurring the lines between different science fields [1]. Indeed, these two distinct yet highly intertwined trends induce a demand of new generation of functional meso scale devices that must have μm-nm resolution and overall size of up to centimeters, pushing existing micro- and nano-manufacturing techniques to their absolute limit. Amidst all of this, 3D printing emerged as a new and powerful manufacturing tool of choice, as it provides nearly limitless structure geometries (within boundaries of resolution) and unmatched idea-to-object realization rate. Optical 3D printing stands out amongst all the 3D

#361084 https://doi.org/10.1364/OE.27.015205
Journal © 2019 Received 6 Mar 2019; revised 25 Apr 2019; accepted 6 May 2019; published 13 May 2019

Optics EXPRESS

printing techniques, as by changing the light source and its parameters a huge variety of different light-matter interaction regimes can be exploited for multi-dimensional free-form structuring [2]. The femtosecond (fs) laser-based 3D laser lithography (3DLL) is the most precise and versatile of those [3, 4] and was used to great effect in fields ranging from micromechanics [5, 6] and biomedicine [7, 8], to integrated micro optics [9, 10] and photonics [11, 12]. Additionally, tinkering with focusing properties [13], applying various interferometry techniques [14] or spatial light modulators [15] allows to tune the resolution and/or structuring rate. Combined with a huge variety of applicable materials [16–18] it makes 3DLL an extremely attractive method for advanced functional structure fabrication.

However, 3DLL is still lacking in some respects which are required for industrial applications of this technology. One of them is an optimal combination of fabrication throughput and size of the final structures. There was always a drive behind making 3DLL structures as large as needed for functional applications without compromising on the achievable resolution [7, 19–24]. This is directly tied to how the material is exposed by the laser beam. In most cases, 3DLL is executed in point-by-point structuring fashion. The exposure is realized either by scanning the laser beam [Fig. 1(a)] or translating the sample in relation to a stationary laser spot [Fig. 1(b)]. In the first case, because of the low inertia of galvanometric scanners, high scanning velocities (up to cm/s) can be achieved. However, this approach is beneficial only while structure size does not exceed the working area of the objective, which in most cases is no more than a few hundred μm. If a larger structure is needed it must be separated into segments, which are then fabricated consecutively. This introduces interfaces between them, called stitches, which reduces the overall integrity of the structure [21–23]. This can be avoided by using linear stages, yet in that case, the translation velocity can potentially introduce the defects due to the inertia. On the other hand, a multi-foci approach via interference pattern or spatial light modulator (SLM) can also be employed to speed up the fabrication process, but that would require additional components in the setup which would increase its complexity. Therefore, at the moment, there is no single solution for making 3D meso scale structures using 3DLL efficiently and without defects or technical difficulties/complications.

Here we present an approach of synchronizing linear stages and galvanometric scanners. The synchronization allows realization of a continuous scan with the working field moving dynamically during manufacturing [Fig. 1(c)]. Fabrication of mm-scale structures without loss in structuring resolution using translation velocities up to cm/s can be realized. Stitching is also avoided. Thus, the inherent weaknesses of each method of scanning are minimized while capitalizing on their strengths. We explain this approach in detail, commenting on its inherent properties. Namely, due to a decreasing energy deposition depth with a stronger free carrier absorption at a larger excitation (pulse energy) and due to dependence of the absorbed energy density solely on the fluence, almost the same width of the polymerised line was observed over several orders of magnitude different scanning speed. We illustrate a potential of this approach by showing a dramatic increase in structuring rate reaching up to 4 orders of magnitude. Finally, example structures are demonstrated with movable parts, scaffolds for regenerative medicine, mm-sized microlenses and photonic crystals. A video showing real time synchronization can be seen in supplementary material [Visualization 1].

2. Materials and methods

As the model material we chose organic-inorganic zirconium containing hybrid pre-polymer SZ2080. It was used as it exhibits minimal shrinkage during fabrication [25], is transparent in all visible part of the light spectrum and is mechanically robust. It was either photosensitized with 1% by weight photoinitiator Irgacure 369 or structured without photoinitiator if that was deemed advantageous for the functionality of a given structure [26]. Sample preparation was as follows: the pre-polymer was drop-casted on a glass slide and then pre-baked to remove the

Optics EXPRESS

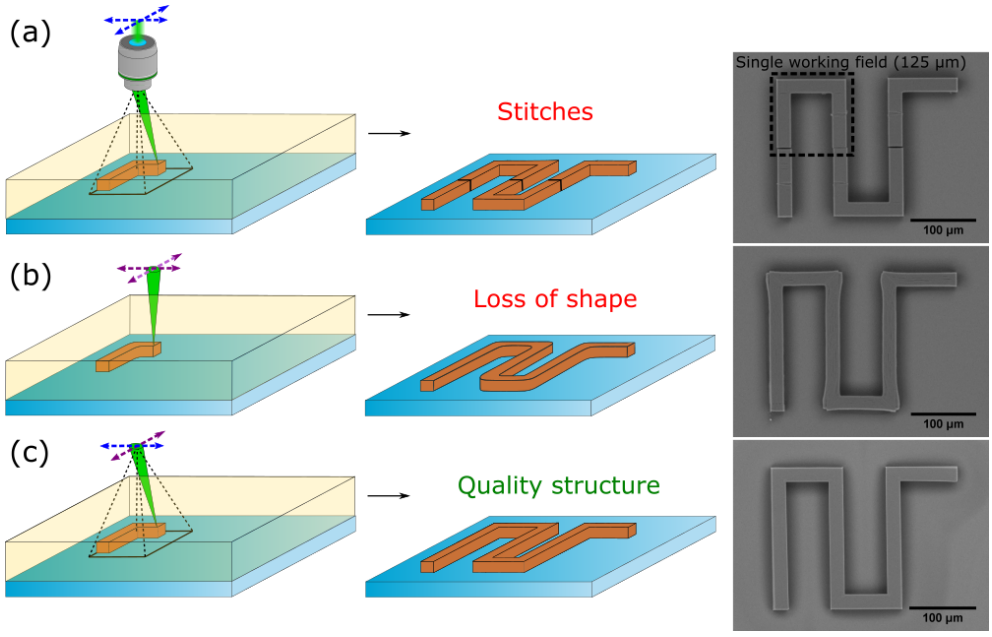

Fig. 1. Principle of producing structures using only galvanometric scanners (a), linear stages (b) and continuous scanning *via* synchronization of both (c). Applying only scanning leads to stitches (black lines on the finished structure) if the size of a structure exceeds the working field of an objective (black square). Linear positioning leads to possible loss of shape (for instance, rounded corners instead of sharp ones) when translation velocity is high (1 mm/s and more) due to stage inertia. Synchronization of both allows to continuously move the working field in relation to the sample thus avoiding stitching yet still exploiting ultra-high speed and precision of structuring by employing scanner. All the given cases are illustrated by the structures fabricated in each regime at 1 cm/s translation velocities.

solvent. After this procedure, the SZ2080 turns into a hard gel and can be exposed to laser radiation. Development was done in isobutyl methyl ketone for 45 minutes.

3DLL was performed using nanopolymerization system in Laser Research Center at Vilnius University and Laser Nanofactory setup in Femtika Ltd. [Fig. 2]. Details on the first setup can be found elsewhere [26]. The Light source in the Laser Nanofactory - laser Pharos (Light Conversion Ltd.) operating at 300 fs pulse duration, 200 kHz repetition rate and 1030 wavelength. Harmonic generator Hiro (Light Conversion Ltd.) converts fundamental wavelength to 515 nm radiation. This wavelength was chosen as it provides a wide processing window for SZ2080 both with and without photoinitiator [26] as well as it has been proven to be suitable for a majority of other commonly used substances in 3DLL lithography [27]. For some structures the photosensitized SZ2080 was also mixed with rhodamine to give it bright purple color and fluorescent properties. In that case, 1030 nm radiation was used for structuring, as 515 would be directly absorbed by the dye (*via* one(-)photon absorption) rendering intricate 3D manufacturing impossible. The laser beam is expanded via 3x telescope to completely fill the objective aperture. Positioning is realized using synchronized linear stages (ANT130XY-160 (Aerotech Inc.)) for XY plane, ANT130LZS-060, (Aerotech Inc.) for Z direction) and galvanometric scanners (AGV-10HPO (Aerotech Inc.)). Real-time imaging of fabrication is done by illuminating the sample with LED and then imaging with a CMOS camera. The whole setup is controlled by 3DPoli software (Femtika Ltd.).

Optics EXPRESS

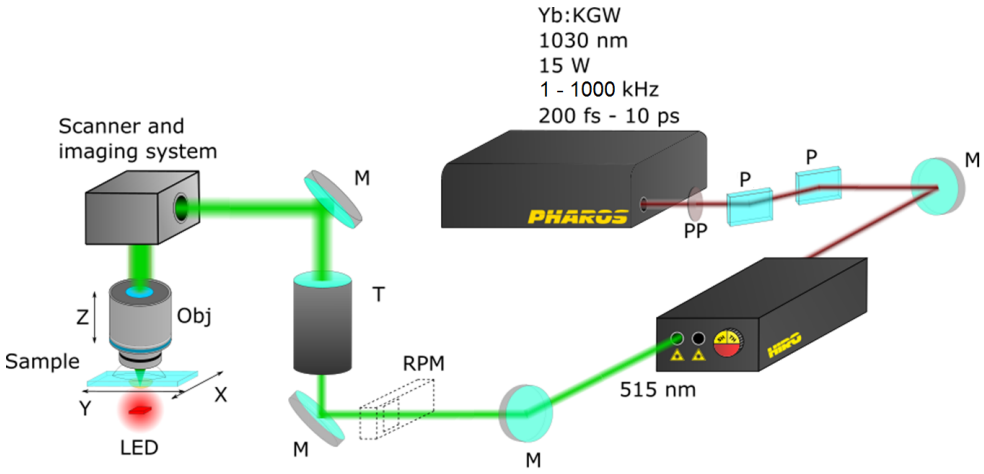

Fig. 2. Schematics of the Laser Nanofactory setup used in this work. Here PP is a phase plate, P denotes thin film polarizers together with PP forming a power attenuation unit, M are the mirrors, RPM - removable power meter, T - telescope, expanding laser beam 3 times, Obj - objective lens. LED illuminates the sample for real-time monitoring of the fabrication process. For wavelength tuning second harmonic crystal, harmonic generator or a parametric generator can be used.

3. Results

3.1. Principles of stage synchronization

3DLL is based on nonlinear interaction between light and pre-polymer, which is confined to the focal point of an objective lens [2]. 3D nano-structure is created by moving the focal point in relation to the sample or *vice versa*. The latter case is achieved by moving the whole sample with various translation stages. These can be based on piezo crystals or other types of linear stages. While piezo positioning is the most precise (up to tenths-of-nm), it is inherently slow and has limited working volume (movement in one direction rarely exceeds a few hundreds of μm). Linear stages, in contrast, can achieve translation velocities up to cm/s while still retaining theoretical precision in the sub-μm range [28]. However, in real world circumstances this is hard to achieve due to inertia accumulated during the fast movement of the device. The larger mass of stage helps to damp vibrational noise which is important for sub-wavelength resolution, however, prohibits fast printing.

In contrast, the focal point can be moved in relation to the sample by using scanners. This can be extremely fast (up to m/s) with minimal limitations to the structuring precision [29]. Its implementation is also relatively simple. For these reasons, it is still a method of choice for the most commercial 3DLL systems. The scanner limitations become apparent when the structure size starts to approach or exceed the working field of the objective lens. In the first case, outer parts of the structured object can become distorted due to various focusing aberrations [30]. Since standard optical objectives are designed for the on-axis imaging at the visible spectral range, aberrations can become severe at near IR wavelengths and larger angles of incidence. If the size of the object is further increased and exceeds the standard working area of high (1.4) NA objectives (up to 150 μm) stitching has to be introduced, further compromising the mechanical and optical qualities of the structure [21–23]. The working field can be increased few-fold by reducing NA, however, at the cost of printing resolution, as the voxels become larger and more elliptical [2].

Optics EXPRESS

In order to overcome these problems, linear stage and galvanometric scanner movement synchronization has to be introduced. The principle behind synchronization can be explained in terms of distributing the translation movements between linear stages and scanners in such a way, that stages are responsible for long and continuous movement, while scanners perform fast movements and/or corrections when needed. This way linear stages have time to both get to the speed and decelerate without causing any defects to the produced structure, as deviations from set translation velocity and trajectory are compensated by the scanners via a feedback loop. The computer capacity of sending information to hardware depends on the geometry since the scanning trajectory has to be adjusted according to the shape complexity and set resolution by splitting it into elemental line sub-structures. Transfer rate is 48 kHz for galvanometric scanners and similar to linear stages - a common frequency for electronics. Thus, it corresponds to a signal sent approximately every 20 μs and at a scanning speed of 10 mm/s it is a trajectory of individual 0.2 μm length lines. This is sufficient, yet increasing the scanning speed up to cm/s would still be suitable for linear structures like woodpiles while limiting the resolution for curved geometries like spirals of small radii. Additionally, the controller has a memory of 100 MB, which is adequate for the employed case but also would be limiting for realization of highly curved structures at high speed unless sacrificing the accuracy.

3.2. Structuring rates

The race to achieve industrial-level manufacturing throughputs pitted different kinds of optical 3D printing methods against each other. While 3DLL is the most accurate one, users of different kinds of optical 3D printing are claiming to be capable of exceeding 3DLL by the volume that can be structured in the same amount of time [31]. However, they have to sacrifice resolution. Just listing translation velocity as the main throughput defining parameter is also insufficient, as it does not specify the size of formed features. Therefore, a lot more sensible way to talk about throughput is by defining the volume of a voxel and structuring rate in terms of voxels per second [24]. In order to calculate these values, we first produced a resolution bridge, where suspended lines were structured with translation velocities v_t of 1, 10, 100, 1000 and 10000 μm/s, speeds that are all now sustainable and usable in repeatable fashion in 3DLL structuring with scanner-stage synchronization. Each suspended line was written using a single laser pass. Average laser power was kept at 10% from the top of fabrication window, i.e. at the power at which controlled polymerization starts to turn into uncontrollable carbonization of the material ("burning") [26]. Exposure conditions during the experiment were: 515 nm wavelength, 300 fs pulse duration, 200 kHz repetition rate. Radial and axial dimensions of voxels are labeled D and L, respectively. Results are given in Fig. 3. An example of the test used to measure D and L is shown in the SEM image in Fig. 3(a). Voxel's dimensions decrease only by a factor of 13 while translation velocity is changed by four orders of magnitude. A comparatively weak dependence of voxel size on scanning speed (exposure dose) results from the efficient crosslinking under single pulse exposure. Under the experimental conditions used in this study, thermal effects and optical filamentation were not contributing to the measured values of D and L. The energy deposition density defining the polymerised volume is shown to be only dependent on the fluence-per-pulse, rather the accumulated dose and scanning velocity (see details in the Discussion section).

Figure 3 presents an experimental evidence that the polymerised voxel size was not dependent on the scan speed, i.e., the exposure dose. Apparently, the length of thermal diffusion, which depends on time t as $\sqrt{t}$ (slope of 0.5) was not defining the size of the voxel. The nonlinear polymerisation would cause the voxel size to evolve with exposure (proportional to the scan speed) with the dependence of slope larger than one. For an eye guide, the slopes separating linear vs. nonlinear as well as thermal diffusion controlled processes are shown with slopes 1 1 and 0.5, respectively. The aspect ratio of the fabricated voxels does not change and is in the range of 3-4, showing that the same scaling is observable in both transverse and longitudinal directions.

Interestingly, other groups showed an opposite trend of the enlargement of the voxel when v_t is increased [32] (see the linear slope for reference in Fig. 3(b)). The difference might lay in the fact, that we used a 200 kHz amplified laser, while the other group used 80 MHz oscillator. This results in negligible distance between pulses in the latter case and distance between pulses reaching up to 50 nm (or around 10% of spot size) in the former when translation v_t is 1 cm/s. Thermal initiation of polymerisation is yet another factor important at high repetition rate [33]. Overall, the achieved resolution is far from minimal of what can be realised with this type of 3DLL system. With the usage of I closer to the bottom of fabrication window a feature size below 400 nm can be easily reached [26]. However, as feature size reduction was not the aim of this study, experiments in this I range were not performed.

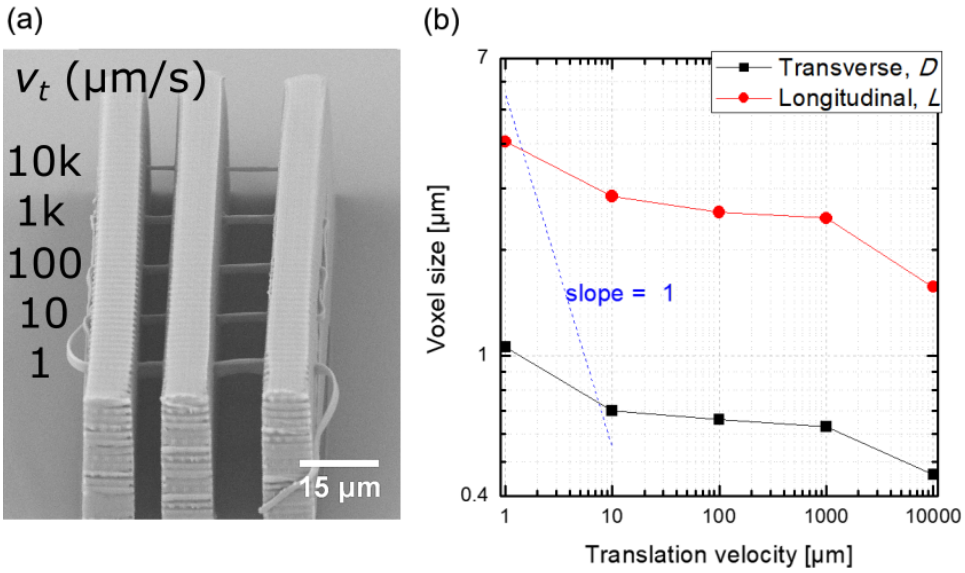

Fig. 3. (a) The resolution bridge fabricated using different translation velocities v_t and measured line widths (b). A sharp decrease in line dimensions is observable. However, the aspect ratio of voxels remains in the 3-4 range. The slope = 1 is shown as an eye guide to illustrate that polymerisation of the voxel was following a sub-linear (slope < 1) power (dose) dependence.

The acquired experimental results can be explained by the numerical modelling of accumulated energy dose shown in Fig. 4. The modeling calculated the entire accumulated energy dose E_t, which accounts to all the single pulse fluences (Gaussian spatial distribution in focal point is assumed) and the movement of the focal plane, i.e. the effect of each pulse having different fluence in every point at every time. The results point out at dramatic difference in threshold (i.e. at line width) E_t as the translation velocity is changed. Specifically, E_t decreases from 545.59 J/cm^2 to 1.98 J/cm^2 when v_t goes from 10 μm/s to 10000 μm/s. Interestingly, at 1 μm/s the line width is substantially larger than the spot diameter ($2w_0$), while in the case of 10000 μm/s it is bellow diffraction limit. This can be interpreted because of continuous excitation of pre-polymer and expansion of polymerization volume in one case and highly contained energy absorption in the other. Also, radicals are generated for an increased amount of time during slower translation velocity, resulting in line broadening as radicals have an immense role in the writing resolution [34].

Optics EXPRESS

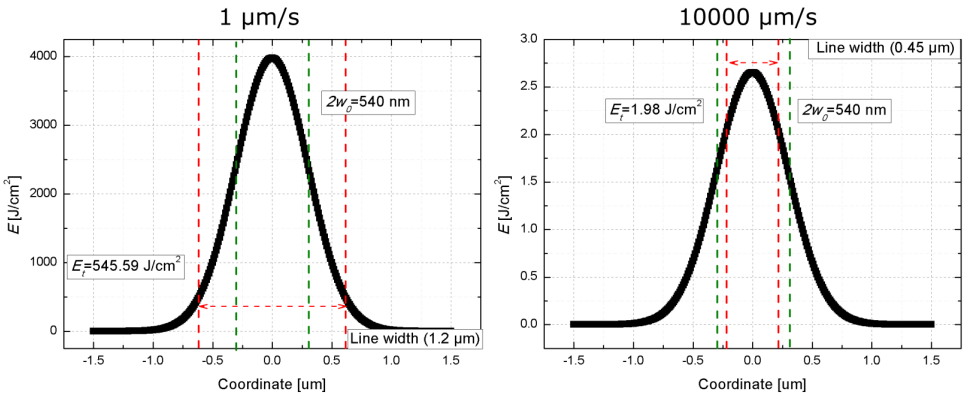

Fig. 4. Plots representing E_t deposition during fs exposure throughout translation of the stages. It is acquired by adding all of the fluences of single pulses dependant on their position during translation and assuming Gaussian distribution. E_t in the centre of the line during formation at v_t of 1 μm/s and 10000 μm/s and 10% below the damage threshold of the polymer. A substantial difference in E_t and the resulting decrease in line width as v_t is higher.

In order to calculate the approximate volume of a voxel, we approximate its shape to the one of an ellipsoid in accordance with the dynamics of voxel formation. Then, the volume of a voxel V_v is [Fig. 5(a)]:

$$V_v = \frac{4}{3}\pi abc = \frac{4}{3}\pi \frac{D}{2}\frac{D}{2}\frac{L}{2} = \frac{1}{6}\pi D^2 L \tag{1}$$

Consequently, we can calculate that volume V_v decreases around 13.7 times when velocity v_t is increased from 1 μm/s to 10000 μm/s [Fig. 5(b)]. While this is a substantial decrease, the v_t increases by 4 orders of magnitude, completely mitigating the possible drop in structuring rate due to the consequentially smaller voxel volume. For instance, if we consider a cube of $1 \times 1 \times 1$ mm^3 size, fabrication times with 1 μm/s and 10000 μm/s are 246903 and 174 hours, respectively. This is a reduction of fabrication time of almost four orders of magnitude when considering a half-voxel overlap in the construction of the cube. Obviously, the dimension of voxels as measured in Fig. 3(b) for 1 μm/s and 10000 μm/s were used in this simple but effective calculation. It can be explained by the increase of the line volume V_l as v_t is raised (following a linear slope rather diffusion defined slope = 0.5 as shown in Fig. 5(c)). The line volume is a volume of a line fabricated at a given translation velocity per unit time. It can be calculated by multiplying the area of the voxel cross-section with the translation velocity, that is V_l=0.25πDLv_t. For example, if a polymerized line is written at a speed of 10 μm/s, its volume in one second is simply 10 μm times the voxel cross-section as measured at that specific translation velocity. Dividing the overall volume of object by the V_l allows calculating manufacturing time of an object (making an assumption that there is no overlap and/or unnecessary movements with closed shutter). Similarly, if V_l is divided by the volume of a single voxel the rate in voxels per second can be uncovered. This way V_l is normalized to V_v giving the rate in voxels per second [Fig. 5(d)]. The gain in throughput is still maintained regardless of the decreasing voxel size. Therefore, maximizing the v_t effectively enhances the overall yield of 3DLL printing. Nevertheless, the existence of the upper limit for V_v will become apparent for a high value of v_t as the polymerization reaction rate will be insufficient for the direct laser writing. Luckily, when we extrapolate V_v for high values of v_t, we notice that this does occur only for tens of cm/s or

Optics EXPRESS

more (for SZ2080 pre-polymer), which are challenging values to achieve for most 3DLL setups even with synchronization.

While structuring rates of voxel volumes per time is a good indicator of expected throughput of 3DLL, real fabrication of complex 3D structures requires some additional considerations. Namely, one must consider voxel overlap required to produce a continuous structure as well as stage movement between different parts of the object.

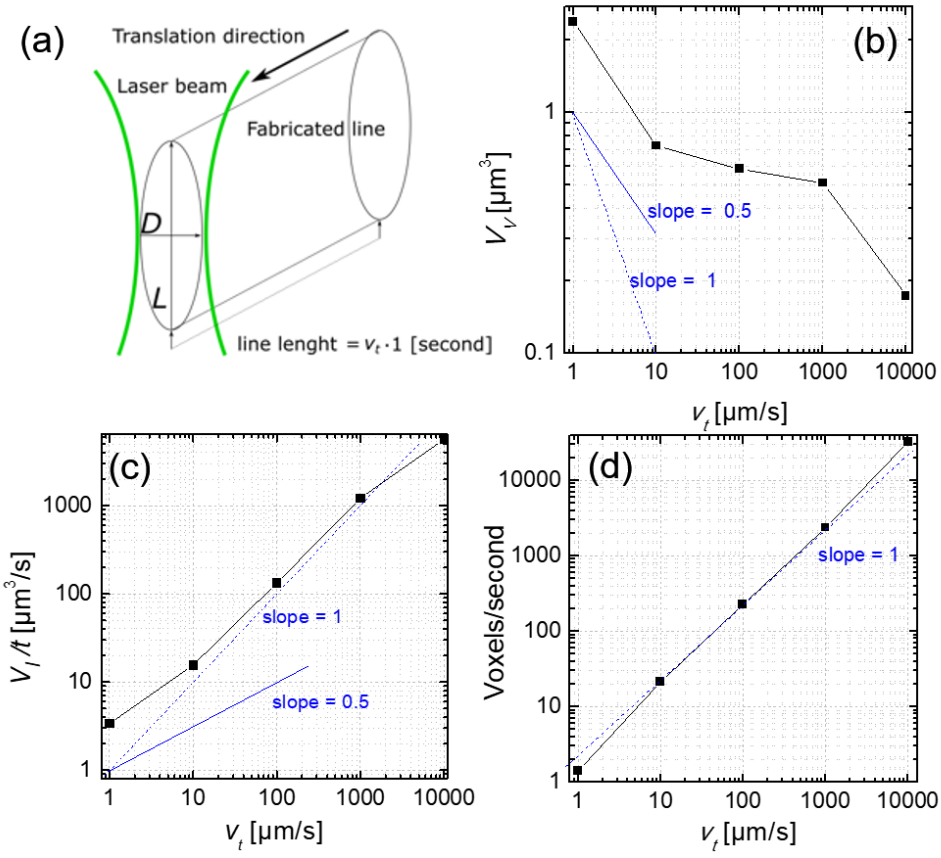

Fig. 5. (a) A schematic representation of a voxel, fabricated line, and definitions of D and L. (b)-(d) are voxel volume V_V, line volume V_l and voxels/second dependencies on the translation velocity v_t respectively. Slopes corresponding to a linear and diffusional spreading (slope = 0.5) of the voxel volume are shown as eye guides. The line volume was proportional (slope = 1) to the scan speed, hence, the exposure dose.

In order to showcase these considerations, we will use gradient chain mail as a model structure. The overall width of the structure is 1 mm, the internal radius of the largest ring is around 100 μm, while the smallest is around 5 μm [Fig. 6(a)]. Support walls are needed in order to attach the ring structure to the glass substrate, yet they can be fabricated with different parameters than the rings (namely lower overlap in the vertical direction) and therefore will be excluded from the discussion.

The STL file of a 3D object is hatched in XY and sliced in Z coordinates, respectively. Which can be independently set to proportional or different steps resulting in the directional fabrication accuracy/throughput. One of the advantages of the control software (3DPoli) is the possibility

Optics EXPRESS

to dynamical change the slicing and hatching steps of different kinds of structures on-the-fly depending on the requirements for the structure fidelity and throughput. The volume of the chain structure is 1280410 μm^3. The structuring rate using v_t = 10000 μm/s is 5667 μm^3/s. Therefore, theoretically, in order to fill all the volume of the object (as shown in Fig. 6(b)), it should take 225 seconds or around 3 and a half minutes. However, in order to achieve a continuous and relatively smooth surface, the slicing and hatching steps of 0.3 μm have to be used, increasing the real structuring duration. Furthermore, there are huge gaps between different parts of the structure, that are covered by the positioning system with a closed laser shutter, creating a lot of movements that do not result in any volume polymerized [Fig. 6(c)]. If this is done in a standard raster scanning fashion using translation stages and galvanometric scanners, the time needed for fabrication is around 2 hours even when synchronization and 1 cm/s v_t are used. If the optimization algorithm is applied minimizing stage movement, the fabrication time can be reduced to 26 minutes. Although this result is impressive, it is still substantially longer than the time given by theoretical calculation.

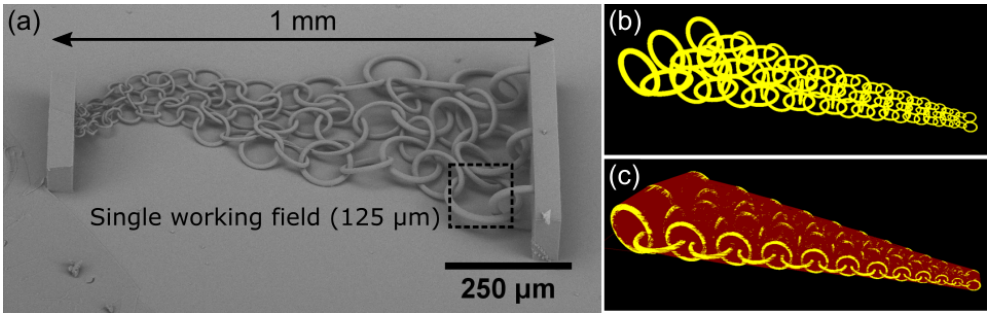

Fig. 6. (a) SEM micrograph of 1 mm long gradient chain-mail (with support walls) showcasing the capability to produce a relatively smooth surface with features that range from μm to hundreds of μm. A single working field of 125 μm is added for the reference, showcasing that the biggest rings would not fit in it. (b) Focal point movements if only the rings would be fabricated. (c) Image showing all the movements needed to produce such structure, including ones with an open shutter (yellow) and with a closed shutter (red). As movements between different parts of the take up a significant portion of the laser beam repositioning between scanning, the time needed to create such structure is 26 minutes, in comparison to 3 and a half minute needed if only the volume will be filledblue.

It is important to note, that theoretically calculated and real fabrication durations converge when the complexity of structure is decreased. For example, if the object is a simple cube, then the number of slicing and hatching steps is minimal. Furthermore, optimization of the production algorithm, for instance, making rings in chain-mail not by linear slicing, but by scanning in circular movements, can further decrease structuring duration. However, limitations apply. For example, the creation of continuous vertical rings by drawing circles in Z direction is impractical, because a shadowing effect would impinge the quality of the ring fragments, as the incident beam path would need to be aligned with already exposed material resulting in beam distortion and overexposure [13].

3.3. Functional meso-scale structures: 3D scaffolds for medicine

Scaffolds for cell growth are playing an increasingly prominent role in the field of regenerative medicine [7, 8]. 3DLL made objects of this kind are especially attractive as the geometry of the scaffold can be custom tailored to best suit the needs of living cells [7]. Coupled with unmatched freedom in choosing the material or combining several of them in one object (so

Optics EXPRESS

called 4D printing) promotes 3DLL as the method of choice in this field [8]. However, medicine requires large numbers of highly repeatable scaffolds, which would be at least a millimeter in size. In order to prove that synchronization of scanners and linear stages can satisfy this demand mm-sized scaffolds for cell growth were manufactured out of pure SZ2080. The overall length of the scaffold was 1.5 mm [Fig. 7(a)]. As results are perfectly reproducible, mass production of objects of this kind is possible [Fig. 7(b)]. Additionally, SZ2080 without photoinitiator was chosen as it should enhance the biocompatibility of the material. Scaffolds of similar size and compatible fill ratio were previously produced by only using linear stages and cm/s level v_t, but it was done with 10x magnification 0.3 NA objective lens exploiting low resolution voxels [35]. By enabling mm-size scaffolds to be produced with high-NA objective a lot more complex and higher-resolution geometries can be achieved, enabling better mimicking of the extracellular matrix which is one of the main requirements for this kind of structures. It is especially relevant as this can also be coupled with an approach of using different focusing conditions for an even greater increase in fabrication throughput. Additionally, 0.8 cm/s speed results in printing time below one hour for such scaffold which is reasonable for structures needed for individual patient orientated regenerative medicine.

3.4. Functional meso-scale structures: refractive microoptics

While integrated micro optics is one of the main driving forces behind 3DLL, most of the structures presented so far in the literature do not exceed a few hundred μm in size [9, 10]. The limiting factors preventing an increase in size are a combination of necessity to use high layer overlap during printing, which is needed in order to achieve surface roughness sufficient for optical use, and a demand for homogeneity of a structure, as any internal defects, for instance stitching, would result in additional scattering and weak points [23]. With continuous scanning both of these problems are eliminated, as high layer overlap in the lens does not cause a massive increase in printing time, as the translation velocity can be in the range between 1 mm/s to 1 cm/s, depending on the quality requirements. Furthermore, stage synchronizations (including in the Z axis) assures that the structure is homogeneous. In this work, 0.5 mm and 1 mm diameter lenses were produced in the time that does not exceed a few hours. SEM analysis showed no significant defects on the surfaces of these objects [Fig. 7(c)]. After measuring focusing properties it was noted that the laser beam formed by such lens in the focal plane is Gaussian-like [Fig. 7(d)]. However, while increasing the size of the lens other fabrication unrelated problems occur. All the polymers used in 3DLL have some degree of inherent shrinkage during fabrication. The material used in this study, SZ2080, was specifically designed with minimal shrinkage [25], yet at these scales even this material could not avoid all the associated problems. 1-2% of shrinkage can be more-less ignored in lenses that are tens-of-μm in size. In mm-sized objects, it becomes an issue that has to be addressed. This requires further work in this direction that is related more to the architecture of the structure, optimized exposure parameters [36] or the material development rather than the fabrication method. All these issues are resolvable by tuned and optimized engineering of exposure.

3.5. Functional meso-scale structures: photonic crystals

One of the possible alternatives to the complex shapes needed in refractive optics would be to use photonic crystals acting as flat optics. While curved refractive optics are sensitive to the position where exactly the light is introduced to the element, in the flat case most of these requirements are neglected. 3DLL is a superb technology for fabrication of such elements, as it is a straightforward process with a possibility to control the line width down to nanometer precision [37]. These elements can be made to provide light controlling capabilities matching or exceeding those of refractive optical elements. The synchronization of stages does not impede the printing resolution or positioning accuracy, thus 1-mm-sized photonic elements consisting of nano-lattices can be

Optics EXPRESS

produced [Fig. 7(e)]. The fabrication time was around 2 hours. A single photonic crystal of this kind has 10 thousand individual rods, arranged into a single lattice consisting of 1.25 million unit cells [Fig. 7(f)]. One point to consider is that optical imaging can only show the surface of the photonic crystal, while the interaction between multiple layers of diffracting lines generates the desired photonic effect. Therefore, in order to prove that the internal structure of a photonic crystal is as designed and not deformed due to increased translation velocity, it was probed by the HeNe laser. Predicted diffractive patterns were observed proving its functionality and superb quality of internal structure [Fig. 7(g)].

3.6. Meso-butterfly

In order to merge all the capabilities demonstrated so far into a single object, a mesoscale butterfly was produced [Fig. 8]. The overall wingspan of the structure reached 1.3 mm, making it clearly visible with the naked eye. Rhodamine was mixed into SZ2080 to dye it bright purple color, at the same time providing functional properties of high-yield fluorescence [38]. The 14 μm thick microcantilever-like antennas were fixed to the head. Eyes consisted of an array of a few-μm-diameter functioning lenses arranged in a semi-random pattern, yet still showing high surface smoothness. As in a real butterfly, wings consisted of nanolattices, which in this case were arranged in the fcc geometry to mimic photonic crystal shown previously. The line width was ~650 nm. The v_t = 1 cm/s combined with dynamic slicing and hatching allowed to achieve printing time of 2.5 hours. Overall it shows true meso-scale capabilities of millimeter-sized structures out of functional material with true nanometer features, and optical-quality level surface roughness in critical areas, such as microlenses. It is important to stress that different parts of the butterfly were produced using the software-enabled dynamic tuning of slicing and hatching steps, with exact parameters given in Table 1. This choice of values can be fully automated enabling on-demand access to different structuring regimes simplifying manufacturing from the user stand point thus making the transition from computer model to the produced structure easy and straightforward.

4. Discussion

Since the dawn of 3DLL technology, the inherent limitation of a point-by-point structuring was recognized and various methods to increase the throughput were suggested. Advanced stitching strategies were employed, yet these can only minimize the adverse effects of this technique [21,39]. Application of interference/structured beams [14] requires substantial changes in the optical layout of the 3DLL setup. Introduction of spatial light modulators (SLM) promised to make light structuring more flexible [15]. However, it further complicated the optical setup and had some inherent limitations in terms of applicable laser power, as in most cases the active matrixes in the SLM are relatively prone to optical damage. Finally, tuning pulse duration was also proposed as a way to decrease the price of the setup, yet it results in dramatic throughput reduction and can be discarded for high-throughput 3DLL systems [31,40]. In contrast, coupling linear stages with scanners is a lot more straightforward solution, the only two components

Table 1. Optimized parameters for fabrication of different parts of the meso-butterfly.

Part	I	v_t	**Slicing**	**Hatching**
Head and top of the body	12.7 TW/cm^2	1 cm/s	0.5 μm	0.2 μm
Body	12.7 TW/cm^2	1 cm/s	2 μm	0.3 μm
Woodpile	12.7 TW/cm^2	1 cm/s	2 μm	2 μm

Optics EXPRESS

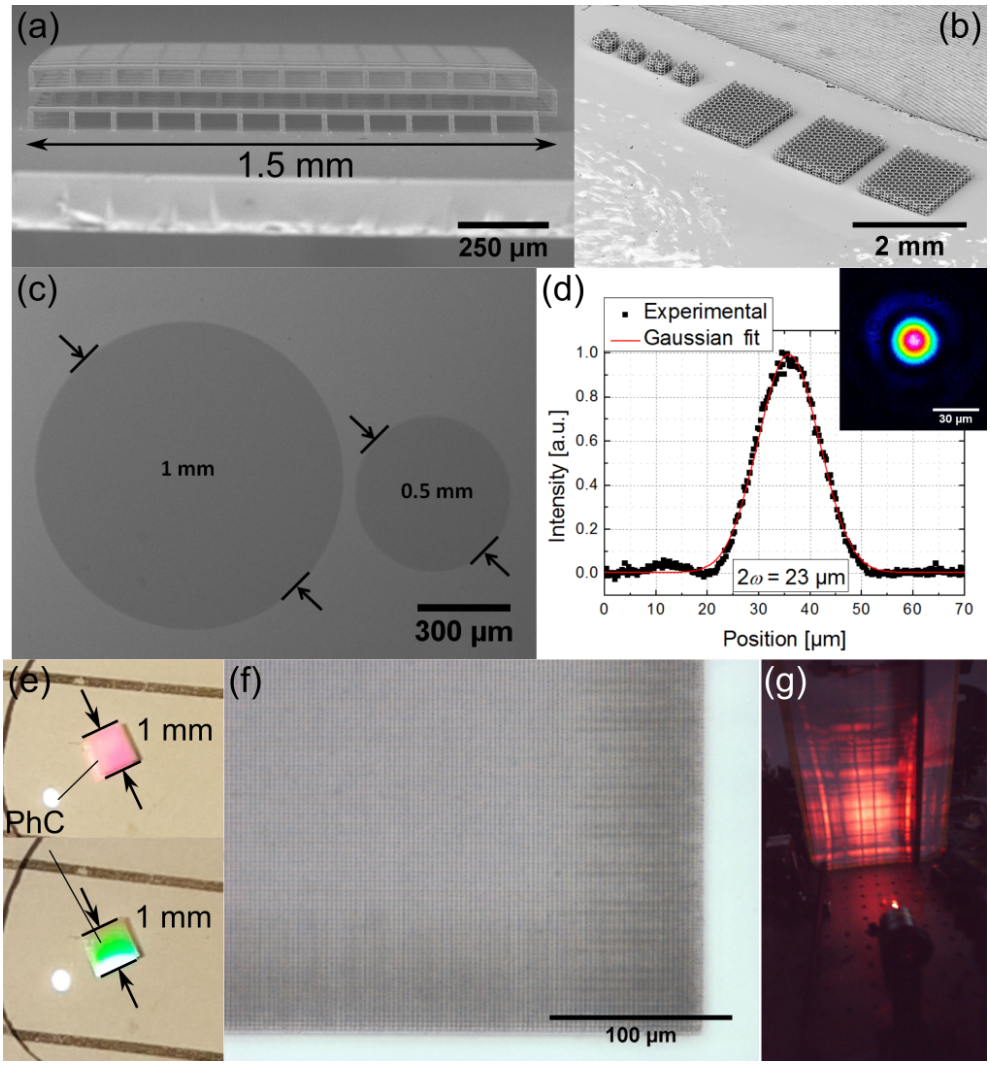

Fig. 7. (a) - 1.5 mm scaffold for cell growth made out of non-photosensitized SZ2080. (b) - demonstration of capabilities to produce complex bio-medicine oriented structures with on-demand scalability (Visualization 1). (c) - SEM images of 0.5 and 1 mm lenses showing no noticeable surface or other defects, as 0.5 mm lens focuses light into a near-perfect Gaussian spot (d). (e) - photos of 1 mm sized photonic crystal before development at different angles in relation to white light illumination, which results in different colours being diffracted towards the photocamera. (f) - optical microscope image of the structure, revealing no defects in the lattice, which is further proved by predictable photonic crystal diffractive pattern projected onto a screen after illumination with HeNe laser beam.

introduced into an optical path are scanners and two lenses arranged in a 4F configuration. As the synchronization and control of the whole operation are performed by digital means, a lot of strain and complexity is removed from the optical part of the system. While it is still a point-by-point structuring method, the relative simplicity makes it an ultimate solution before active on-the-go light structuring *via* SLM can be introduced at-large.

Indeed, the essential idea of combining fast beam deflection with a wide field of translation

Optics EXPRESS

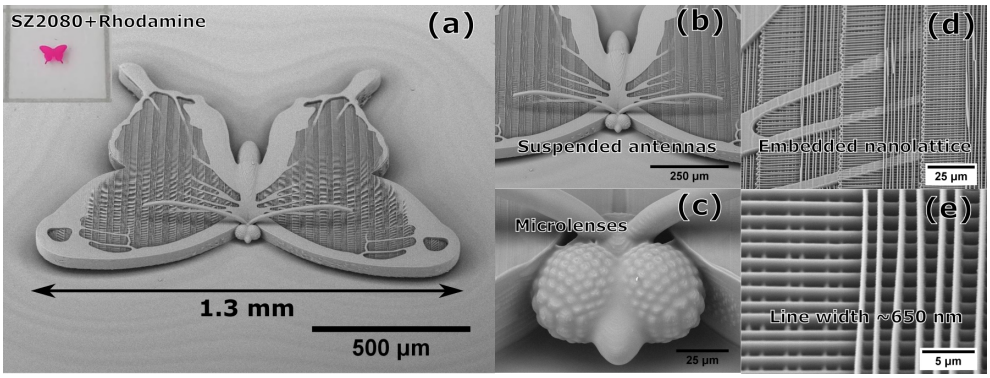

Fig. 8. A mesoscale butterfly, created to demonstrate true meso-scale capabilities of synchronized linear stages and galvanometric scanners. (a) - an overall SEM view with a naked-eye view in the inset. (b) - enlarged view of suspended antennas. (c) - eye microlens array. (d) shows embedded nanolattice with a single line width of 650 nm (e).

stages is a rather generic one and has been foreseen by several research groups and being developed by industrial companies, yet up to know was not implemented for the true 3D writing. Namely, planar lithographic processing was first introduced in 1989 [41] and significantly advanced by in 2006 [42] by enabling vertical stacking of individual layers empowering direct CAD-CAM fabrication [43]. However, these solutions were still restricted to a combination of just planar or sequential layer-by-layer volumetric processing. Here we show a conceptually novel approach for continuous three-dimensional direct laser writing for literally geometry-unrestricted precision 3D additive manufacturing.

From a technological point of view, this study was made possible essentially by use of the electronics and software capable of synchronizing galvanometric mirrors with stages. Exploiting the transfer rate of 48 kHz (signal every 20 μs) and at a scanning speed of up to 10 mm/s it is realizing a trajectory of connected individual 0.2 μm length lines. This coincides well with the experimentally deduced hatching step of 0.3 μm used for fabricating gradient chain-mail and mesoscale butterfly (bulk part). Meanwhile the microlenses were manufactured using hatching step of 0.02 μm with translation velocity of 2 mm/s. Applying the same estimations one can see the inter-signal distance is 0.04 μm. Therefore, advances in electronic data transfer between devices are obligatory in order to further increase the speed for next-generation high-resolution continuous writing setups.

Currently, the meso-scale structures are highly desired in many different fields, as they allow to introduce micro- or even nano-level interactions into a macro-sized object. So far 2D and 2.5D fabrications in this scale have been achieved by employing various lithographic technologies. However, true 3D structures are not easy to achieve. As 3DLL can be combined with other manufacturing techniques and structures can be produced on [9] or in [44] various substrates, elimination of stitching without sacrificing speed or fidelity of printing is highly promising. Additionally, if a highly tunable amplified femtosecond laser system is used capabilities of synchronization can be extended into subtractive manufacturing as well. In that case, *via* welding, laser-assisted etching or ablation, highly complex structures can be made [45, 46]. Combining an amplified fs laser with a synchronization-capable positioning system enables a single manufacturing setup for highly complex, multi-material structures.

Furthermore, the capability to perform laser fabrication with translation velocities exceeding 1 cm/s allows having a new way of investigating the fundamentals of light-matter interaction. 3D laser polymerization is defined by light absorption in the focal volume, hence, volumetric

Optics EXPRESS

absorbed energy density J/cm^3. The resolution of 3D fabrication is determined by the volumetric localization of that energy, which depends on the optical or/and thermal localization within the volume where the threshold of modification is exceeded. The modification is broadly defined by phase transitions (melting, evaporation, plasma formation), ablation, or (de)polymerization depending of the host material.

The direct energy deposition by ultra-short laser pulses can be analyzed by X-ray emission *via* bremsstrahlung in plasma created at the focus [47]. X-ray intensity is proportional to the absorbed energy at the interface with a solid or liquid target while the black body radiation contribution at the longer times after the pulse has a minor contribution. The spatial localization of absorbed energy in all three dimensions is estimated next. The skin depth (for the the E-field) of the optically excited material is determined by the imaginary part of the refractive index $n \equiv \sqrt{\varepsilon} = n + i\kappa$ as $l_{abs} = c/(\omega\kappa) = \lambda/(2\pi\kappa)$, it is $l_{abs}/2$ for the intensity $I \propto E^2$. The lateral dimension of the energy deposition is defined by the focal spot diameter which can be estimated as $2w_0 = 1.22\lambda/NA$ for the wavelength λ and the numerical aperture NA of the focusing lens. The depth-of-focus usually estimated via the Rayleigh length, z_R, as $2z_R = 2\pi w_0^2/\lambda$ is much larger than the actual depth of energy deposition (the skin depth), l_{abs}. This is the key difference for the nonlinear energy deposition.

The absorbed energy density per volume [J/cm^3] at the end of the laser pulse is $W_{abs} = 2AF_p/l_{abs}$, where the integral fluence per pulse is $F_p = \int_0^{t_p} I(t)dt$, A is the absorbance defined by the instantaneous value of the permittivity, $I(t)$ is the temporal envelope of the intensity [48]. At the pre-breakdown conditions in dielectrics when the real part of permittivity $\Re\varepsilon \to 0$, the change of the imaginary part of permittivity is given by [48]:

$$(\Delta\varepsilon_d)_{im} \simeq \frac{\omega_{pe}^2}{\omega^2}\frac{\nu_e}{\omega} = \frac{n_e}{n_{cr}}\frac{\nu_e}{\omega}, \tag{2}$$

where $\omega_{pe} = \sqrt{4\pi e^2 n_e/m_e}$ is the cyclic electron plasma frequency, e, m_e are the electron charge and mass, respectively, n_e is the electron density, ν_e is the electron relaxation frequency (electron-phonon in solid state material), $n_{cr} = \omega^2 m_e/(4\pi e^2)$ is the critical plasma density which was 4.21×10^{21} cm^{-3} at the $\lambda = 515$ nm wavelength in this study. The permittivity at the pre-breakdown in dielectric medium is $\varepsilon_d \simeq n_0^2 + i \times (\Delta\varepsilon_d)_{im} = n_0^2 + i2n_0\kappa$, where n_0 is the real part of an unperturbed refractive index [48]. Hence, the skin depth with the use of Eqn. 2 can be expressed as [48]:

$$l_{abs} = \frac{\lambda}{2\pi\kappa} = \frac{n_0\lambda}{\pi(\Delta\varepsilon_d)_{im}} = \frac{2cn_0}{\nu_e}\frac{n_{cr}}{n_e} \tag{3}$$

and is defining the depth (axial) localization of the energy deposition. The absorbed energy density over the focal spot:

$$W_{abs} = A_0\frac{\nu_e}{cn_0}\frac{n_e}{n_{cr}}F_p \propto \frac{n_e}{n_{cr}}F_p, \tag{4}$$

where the unperturbed absorbance $A_0 \equiv 4n_0/[(n_0+1)^2 + \kappa^2] \simeq 4n_0/(n_0+1)^2$ is neglecting the imaginary part of the refractive index, κ. Equation 4 shows that as the electron density, n_e, is approaching critical, the most efficient energy deposition occurs since the $\frac{n_e}{n_{cr}}$ approach the maximum value of unity.

For the nonlinear absorption via $n-$photon process, the generation of electrons $n_e \propto I_p^n \sim F_p^n$. It begins to saturate as the critical density, n_{cr}, is approached and the breakdown region behaves metal-like. The absorbed energy in the skin layer is proportional to the fluence, $W_{abs} \sim F_p$.

From the scaling shown above (Eqn. 4), the role of strong pulse accumulation and changes of material absorption a larger energy deposition occurs. The nonlinearity of energy deposition is decreasing as $n_e \to n_{cr}$. This leads to saturation. In the case of X-ray emission under two-pulse

excitation [47], the absorbed energy per volume (Eqn. 4) was driven by a linear process of electron generation $W_{abs} \sim n_e \times F_p \propto F_p^2$ and the power scaling showed the expected $\gamma = 2$ slope for the one-photon absorption. This behavior is expected to be generic when the observed characteristic of light-matter interaction depends on the pre-excitation (n_e in the analysis above). We put forward a conjecture, that in the case of laser polymerization and strong pulse-to-pulse overlap we expect this behavior. Thermal accumulation is also usually increasing the imaginary part of permittivity.

Next, pulse-to-pulse overlap at the increasing scan speed, v_t, has to be discussed. It should lead to the linear scaling of $W_{abs} \sim F_p$ since the faster speed should cause proportionally smaller excitation, i.e., $n_e \sim v_t^{-1}$. This explains the experimentally observed weak dependence of the polymerised line width on the scanning velocity [Fig. 3].

According to the experimental results, a numerical modelling of exposure was carried out [Fig. 4]. The results point out at dramatic difference in threshold (i.e. at line width) energy dose accumulation (E_t) in both cases (545.59 J/cm^2 vs 1.98 J/cm^2). Interestingly, at 1 μm/s the line width is substantially larger than the spot diameter ($2w_0$), while in the case of 10000 μm/s it is bellow diffraction limit.

5. Conclusions

In this work, the possibility to adopt synchronized linear stages and galvanometric scanners for meso-scale 3D structure additive manufacturing was shown. It allowed achieving linear translation velocities in the range of cm/s and provide stitch-free structuring. Peculiarities of polymerization with translation velocities from 1 μm/s to 1 cm/s were uncovered, showing that while inter-pulse distance reaches up to 50 nm (i.e. around 10% of spot size of 1.4 NA objective with 515 nm wavelength) at 200 kHz repetition rate, polymerization is still homogeneous enabling fabrication of robust features with sizes down to 460 nm. It is shown that the volume density of the absorbed light was defining the width of the 3D polymerised lines and was depended on the pulse fluence rather the exposure dose and scanning speed. This resulted in individual voxel volumes of 0.17 μm^3 and structuring rate of 32609 voxels/s. In order to demonstrate the potency of this approach functional structures for biomedicine, micro optics and photonics were produced.

Finally, it was all successfully combined in a benchmark 1.3 mm wingspan mesoscale butterfly, featuring cantilever-like antennas, eyes of microlenses and photonic crystal-like woodpiles within the wings. Overall, the presented findings paint a bright future for the synchronization-based 3DLL as high-throughput stitch-free manufacturing is crucial for various fields dependent on on-demand printing of functional micro- and nano-devices. The performed demonstration proves the femtosecond laser 3D nanolithography (also known as TPP, 2PP, MPP or non-linear one) is no longer limited to fabrication of just small sample structures or stitched bigger objects which inherit anisotropic shrinkage. The proposed method can be applied to a variety of materials (including inorganic ones [49, 50]) processed *via* lithography routes.

Funding

NATO Science for Peace and Security program's project "*Nanostructures for Highly Efficient Infrared Detection*" SPS-985048; European Commission's Seventh Framework Programme Laserlab-Europe IV JRA support BIOAPP (EC-GA 654148); Research Council of Lithuania (LMTLT) project "+tech-" (S-MIP-17-99); Australian Research Council grant DP190103284.

Acknowledgments

Authors would like to acknowledge the technical support, modeling and measuring work performed by Mr. Tomas Baravykas (Femtika Ltd.). We would also like to thank Prof. Aleksandr Ovsianikov

Optics EXPRESS

(TU Wien) for insightful discussions about terminology behind continuous writing.

References

1. H. Lasi, P. Fettke, H. G. Kemper, T. Feld, and M. Hoffman, "Industry 4.0," Bus. Inf. Syst. Eng. **6**, 239–242 (2014).
2. L. Jonušauskas, S. Juodkazis, and M. Malinauskas, "Optical 3D printing: bridging the gaps in the mesoscale," J. Opt. **20**, 053001 (2018).
3. Y. L. Zhang, Q. D. Chen, H. Xia, and H. B. Sun, "Designable 3D nanofabrication by femtosecond laser direct writing," NanoToday **5**, 435–448 (2010).
4. M. Malinauskas, A. Žukauskas, S. Hasegawa, Y. Hayasaki, V. Mizeikis, R. Buividas, and S. Juodkazis, "Ultrafast laser processing of materials: from science to industry," Light. Sci. Appl. **5**, e16133 (2016).
5. C. Schizas, V. Melissinaki, A. Gaidukevičiūtė, C. Reinhardt, C. Ohrt, V. Dedoussis, B. N. Chichkov, M. F. C. Fotakis, and D. Karalekas, "On the design and fabrication by two-photon polymerization of a readily assembled micro-valve," Int. J. Adv. Manuf. Technol. **48**, 435–441 (2010).
6. T. Frenzel, M. Kadic, and M. Wegener, "Three-dimensional mechanical metamaterials with a twist," Science **358**, 1072–1074 (2017).
7. J. Mačiulaitis, M. Deveikytė, S. Rekštytė, M. Bratchikov, A. Darinskas, A. Šimbelytė, G. Daunoras, A. Laurinavičienė, A. Laurinavičius, R. Gudas, M. Malinauskas, and R. Mačiulaitis, "Preclinical study of SZ2080 material 3D microstructured scaffolds for cartilage tissue engineering made by femtosecond direct laser writing lithography," Biofabrication **7**, 015015 (2015).
8. B. Richter, V. Hahn, S. Bertels, T. K. Claus, M. Wegener, G. Delaittre, C. Barner-Kowollik, and M. Bastmeyer, "Guiding cell attachment in 3D microscaffolds selectively functionalized with two distinct adhesion proteins," Adv. Mater. **29**, 1604342 (2017).
9. T. Gissibl, S. Thiele, A. Herkommer, and H. Giessen, "Two-photon direct laser writing of ultracompact multi-lens objectives," Nat. Photonics **10**, 554–560 (2016).
10. P.-I. Dietrich, M. Blaicher, I. Reuter, M. Billah, T. Hoose, A. Hofmann, C. Caer, R. Dangel, B. Offrein, U. Troppenz, M. Moehrle, W. Freude, and C. Koos, "In situ 3D nanoprinting of free-form coupling elements for hybrid photonic integration," Nat. Photonics **12**, 241–247 (2018).
11. A. I. Aristov, M. Manousidaki, A. Danilov, K. Terzaki, C. Fotakis, M. Farsari, and A. V. Kabashin, "3D plasmonic crystal metamaterials for ultra-sensitive biosensing," Sci. Rep. **6**, 25380 (2016).
12. T. Koschny, C. M. Soukoulis, and M. Wegener, "Metamaterials in microwaves, optics, mechanics, thermodynamics, and transport," J. Opt. **9**, 084005 (2017).
13. L. Jonušauskas, S. Rekštytė, and M. Malinauskas, "Augmentation of direct laser writing fabrication throughput for three-dimensional structures by varying focusing conditions," Opt. Eng. **53**, 125102 (2014).
14. M. Garliauskas, E. Stankevičius, and G. Račiukaitis, "Laser intensity-based geometry control of periodic submicron polymer structures fabricated by laser interference lithography," Opt. Express **7**, 179–184 (2017).
15. L. Yang, A. El-Tamer, U. Hinze, J. Li, Y. Hu, W. Huang, J. Chu, and B. N. Chichkov, "Parallel direct laser writing of micro-optical and photonic structures using spatial light modulator," Opt. Lasers Eng. **70**, 26–32 (2015).
16. M. Farsari, M. Vamvakaki, and B. N. Chichkov, "Multiphoton polymerization of hybrid materials," J. Opt. **12**, 124001 (2010).
17. C. Barner-Kowollik, M. Bastmeyer, E. Blasco, G. Delaittre, P. Muller, B. Richter, and M. Wegener, "3D laser micro- and nanoprinting: Challenges for chemistry," Angew. Chem. Int. Ed. **56**, 15828–15845 (2017).
18. M. Lebedevaitė, J. Ostrauskaitė, E. Skliutas, and M. Malinauskas, "Photoinitiator free resins composed of plant-derived monomers for the optical μ-3D printing of thermosets," Polymers **11**, 116 (2019).
19. Y.-L. Sun, W.-F. Dong, L.-G. Niu, T. Jiang, D.-X. Liu, L. Zhang, Y.-S. Wang, Q.-D. Chen, D.-P. Kim, and H.-B. Sun, "Protein-based soft micro-optics fabricated by femtosecond laser direct writing," Light. Sci. Appl. **3**, e129 (2014).
20. L. Jiang, W. Xiong, Y. Zhou, Y. Liu, X. Huang, D. Li, T. Baldacchini, L. Jiang, and Y. Lu, "Performance comparison of acrylic and thiol-acrylic resins in two-photon polymerization," Opt. Express **24**, 13687–13701 (2016).
21. J. S. Oakdale, R. F. Smith, J.-B. Forien, W. L. Smith, S. J. Ali, L. B. Bayu Aji, T. M. Willey, J. Ye, A. W. van Buuren, M. A. Worthington, S. T. Prisbrey, H. S. Park, P. A. Amendt, T. F. Baumann, and J. Biener, "Direct laser writing of low-density interdigitated foams for plasma drive shaping," Adv. Funct. Mater. **27**, 1702425 (2017).
22. A. Accardo, M.-C. Blatché, R. Courson, I. Loubinoux, C. Thibault, L. Malaquin, and C. Vieu, "Multiphoton direct laser writing and 3D imaging of polymeric freestanding architectures for cell colonization," Small **13**, 1700621 (2017).
23. H. Ni, G. Yuan, L. Sun, N. Chang, D. Zhang, R. Chen, L. Jiang, H. Chen, Z. Gu, and X. Zhao, "Large-scale high-numerical-aperture super-oscillatory lens fabricated by direct laser writing lithography," RSC Adv. **8**, 20117–20123 (2018).
24. A. Vyatskikh, S. Delalande, A. Kudo, X. Zhang, C. M. Portela, and J. R. Greer, "Additive manufacturing of 3D nano-architected metals," Nat. Commun. **9**, 593 (2018).
25. A. Ovsianikov, J. Viertl, B. Chichkov, M. Oubaha, B. MacCraith, I. Sakellari, A. Giakoumaki, D. Gray, M. Vamvakakian, M. Farsari, and C. Fotakis, "Ultra-low shrinkage hybrid photosensitive material for two-photon polymerization microfabrication," ACS Nano **2**, 2257–2262 (2008).
26. L. Jonušauskas, D. Gailevičius, L. Mikoliūnaitė, D. Sakalauskas, S. Šakirzanovas, S. Juodkazis, and M. Malinauskas, "Optically clear and resilient free-form μ-optics 3D-printed via ultrafast laser lithography," Materials **10**, 12 (2017).

Optics EXPRESS

27. M. Malinauskas, V. Purlys, M. Rutkauskas, A. Gaidukevičiūtė, and R. Gadonas, "Femtosecond visible light induced two-photon photopolymerization for 3D micro/nanostructuring in photoresists and photopolymers," Lith. J. Phys **50**, 201–207 (2010).
28. J. Torgersen, A. Ovsianikov, V. Mironov, N. Pucher, X. Qin, Z. Li, K. Cicha, T. Machacek, R. Liska, V. Jantsch, and J. Stampfl, "Photo-sensitive hydrogels for three-dimensional laser microfabrication in the presence of whole organisms," J. Biomed. Opt. **17**, 105008 (2012).
29. N. Alharbi, R. Osman, and D. Wismeijer, "Effects of build direction on the mechanical properties of 3D-printed complete coverage interim dental restorations," J. Prosthet. Dent. **115**, 760–767 (2016).
30. J. Ai, M. Lv, M. Jiang, J. Liu, and X. Zeng, "Focused laser lithographic system for efficient and cross-scale fabrication of large-area and 3D micro-patterns," Opt. Lasers Eng. **107**, 335–341 (2018).
31. X. Chen, W. Liu, B. Dong, J. Lee, H. O. T. Ware, H. F. Zhang, and C. Sun, "High-speed 3D printing of millimeter-size customized aspheric imaging lenses with sub 7 nm surface roughness," Adv. Mater. **30**, 1705683 (2018).
32. E. Waller and G. Freymann, "Spatio-temporal proximity characteristics in 3D μ-printing via multi-photon absorption," Polymers **8**, 297 (2016).
33. M. Malinauskas, P. Danilevičius, and S. Juodkazis, "Three-dimensional micro-/nano-structuring via direct write polymerization with picosecond laser pulses," Opt. Express **19**, 5602–5610 (2011).
34. I. Sakellari, E. Kabouraki, D. Gray, V. Purlys, C. Fotakis, A. Pikulin, N. Bityurin, M. Vamvakaki, and M. Farsari, "Diffusion-assisted high-resolution direct femtosecond laser writing," ACS Nano **6**, 2302–2311 (2012).
35. P. Danilevičius, S. Rekštytė, E. Balčiūnas, A. Karaniauskas, R. Širmenis, D. Baltriukienė, M. Malinauskas, V. Bukelskienė, R. Gadonas, V. Sirvydis, and A. Piskarskas, "Direct laser fabrication of polymeric implants for cardiovascular surgery," Mater. Sci. **18**, 145–149 (2012).
36. A. Žukauskas, I. Matulaitienė, D. Paipulas, G. Niaura, M. Malinauskas, and R. Gadonas, "Tuning the refractive index in 3D direct laser writing lithography: towards GRIN microoptics," Laser Photonics Rev. **9**, 706–712 (2015).
37. S. Rekštytė, T. Jonavičius, D. Gailevičius, M. Malinauskas, V. Mizeikis, E. G. Gamaly, and S. Juodkazis, "Nanoscale precision of 3D polymerization via polarization control," Adv. Opt. Mater. **4**, 1209–1214 (2016).
38. A. Žukauskas, M. Malinauskas, L. Kontenis, V. Purlys, D. Paipulas, M. Vengris, and R. Gadonas, "Organic dye doped microstructures for optically active functional devices fabricated via two-photon polymerization technique," Lith. J. Phys. **50**, 55–61 (2010).
39. S. Dehaeck, B. Scheid, and P. Lambert, "Adaptive stitching for meso-scale printing with two-photon lithography," Addit. Manuf. **21**, 589–597 (2018).
40. M. T. Do, T. T. N. Nguyen, Q. Li, H. Benisty, I. Ledoux-Rak, and N. D. Lai, "Submicrometer 3D structures fabrication enabled by one-photon absorption direct laser writing," Opt. Express **21**, 20964–20973 (2013).
41. C. Rensch, S. Hell, M. v. Schickfus, and S. Hunklinger, "Laser scanner for direct writing lithography," Appl. Opt. **28**, 3754–3758 (1989).
42. L. Cunningham, M. Veilleux, and P. Campagnola, "Freeform multiphoton exicted microfabrication for biological applications using a rapid prototyping CAD-based approach," Opt. Express **14**, 8613–8621 (2006).
43. R. Nielson, B. Kaehr, and J. Shear, "Microreplication and design of biological architectures using dynamic-mask multiphoton lithography," Small **5**, 120–125 (2009).
44. D. Wu, S.-Z. Wu, J. Xu, L.-G. Niu, K. Midorikawa, and K. Sugioka, "Hybrid femtosecond laser microfabrication to achieve true 3D glass/polymer composite biochips with multiscale features and high performance: the concept of ship-in-a-bottle biochip," Laser Photonics Rev. **8**, 458–467 (2014).
45. L. Jonušauskas, S. Rekštytė, R. Buividas, S. Butkus, R. Gadonas, S. Juodkazis, and M. Malinauskas, "Hybrid subtractive-additive-welding microfabrication for lab-on-chip (LOC) applications via single amplified femtosecond laser source," Opt. Eng. **56**, 094108 (2017).
46. T. Tičkūnas, M. Perrenoud, S. Butkus, R. Gadonas, S. Rekštytė, M. Malinauskas, D. Paipulas, Y. Bellouard, and V. Sirutkaitis, "Combination of additive and subtractive laser 3D microprocessing in hybrid glass/polymer microsystems for chemical sensing applications," Opt. Express **25**, 26280–26288 (2017).
47. W.-H. Hsu, F. C. P. Masim, A. Balčytis, S. Juodkazis, and K. Hatanaka, "Dynamic position shifts of X-ray emission from a water film induced by a pair of time-delayed femtosecond laser pulses," Opt. Express **25**, 24109–24118 (2017).
48. E. G. Gamaly, *Femtosecond Laser-Matter Interaction: Theory, Experiments and Applications* (Pan Stanford, Singapore, 2011), 1st ed.
49. D. Gailevičius, V. Padolskytė, L. Mikoliūnaitė, S. Šakirzanovas, S. Juodkazis, and M. Malinauskas, "Additive-manufacturing of 3D glass-ceramics down to nanoscale resolution," Nanoscale Horiz. **4**, 647 (2019).
50. A. Rodenas, M. Gu, G. Corrielli, P. Paie, S. John, A. Kar, and R. Osellame, "Three-dimensional femtosecond laser nanolithography of crystals," Nat. Photon. **13**, 105–109 (2019).